Radiocarbon, Vol 00, Nr 00, 2022, p 1–16 DOI:10.1017/RDC.2022.83

A MODERN MULTICENTENNIAL RECORD OF RADIOCARBON VARIABILITY FROM AN EXACTLY DATED BIVALVE CHRONOLOGY AT THE TREE NOB SITE (ALASKA COASTAL CURRENT)

David C Edge[1]* • Alan D Wanamaker[2] • Lydia M Staisch[3] • David J Reynolds[4] • Karine L Holmes[2] • Bryan A Black[1]

[1]Laboratory of Tree Ring Research, University of Arizona, Bryant Bannister Tree Ring Building, 1215 E Lowell St, Tucson, AZ 85721, USA
[2]Department of Geological and Atmospheric Sciences, Iowa State University, 2237 Osborn Dr, Ames, IA 50011, USA
[3]Geology, Minerals, Energy, and Geophysics Science Center, United States Geological Survey, Moffett Field - Building 19, 345 Middlefield Road MS973, Menlo Park, CA 94025, USA
[4]Centre for Geography and Environmental Science, Department of Earth and Environmental Science, University of Exeter, Penryn Campus, Treliever Road, Penryn, Cornwall, TR10 9FE, UK

ABSTRACT. Quantifying the marine radiocarbon reservoir effect, offsets (ΔR), and ΔR variability over time is critical to improving dating estimates of marine samples while also providing a proxy of water mass dynamics. In the northeastern Pacific, where no high-resolution time series of ΔR has yet been established, we sampled radiocarbon (^{14}C) from exactly dated growth increments in a multicentennial chronology of the long-lived bivalve, Pacific geoduck (*Paneopea generosa*) at the Tree Nob site, coastal British Columbia, Canada. Samples were taken at approximately decadal time intervals from 1725 CE to 1920 CE and indicate average ΔR values of 256 ± 22 years (1σ) consistent with existing discrete estimates. Temporal variability in ΔR is small relative to analogous Atlantic records except for an unusually old-water event, 1802–1812. The correlation between ΔR and sea surface temperature (SST) reconstructed from geoduck increment width is weakly significant (r^2 = .29, p = .03), indicating warm water is generally old, when the 1802–1812 interval is excluded. This interval contains the oldest (–2.1σ) anomaly, and that is coincident with the coldest (–2.7σ) anomalies of the temperature reconstruction. An additional 32 ^{14}C values spanning 1952–1980 were detrended using a northeastern Pacific bomb pulse curve. Significant positive correlations were identified between the detrended ^{14}C data and annual El Niño Southern Oscillation (ENSO) and summer SST such that cooler conditions are associated with older water. Thus, ^{14}C is generally relatively stable with weak, potentially inconsistent associations to climate variables, but capable of infrequent excursions as illustrated by the unusually cold, old-water 1802–1812 interval.

KEYWORDS: ΔR chronology, northeast pacific, paleoceanography, sclerochronology.

INTRODUCTION

Radiocarbon (^{14}C) is produced in the upper atmosphere from the interaction between cosmic radiation and nitrogen atoms, and due to its predictable rate of decay, is widely used as a geochronometer for dating organic material (e.g., Schuur et al. 2016). The rate of ^{14}C production, however, varies over time, as has been quantified by measuring levels in exactly dated tree rings over the past several millennia (Stuiver et al. 1986a). Information on this year-to-year variability in atmospheric ^{14}C is now used to increase dating accuracy (Büntgen et al. 2018; Pearson et al. 2020; Reimer et al. 2020). In the marine system, ^{14}C dating is complicated by the time necessary for atmospheric ^{14}C to equilibrate across surface-ocean environments. Dating is further complicated due to the mixing of water masses, some of which may have been isolated from the surface and therefore relatively depleted in ^{14}C (Stuiver et al. 1986b). This so-called marine radiocarbon reservoir effect (Stuiver et al. 1986b; Alves et al. 2018) can add 1000 or more years of uncertainty to dating estimates and varies considerably over a range of spatial scales. In the northeast (NE) Pacific north of 40°N, average radiocarbon ages are 600–1000 years older than contemporaneous terrestrial samples (McNeely et al. 1991). Significant spatial heterogeneity

*Corresponding author. Email: dedge@arizona.edu

in ^{14}C content has been observed on the order of 200 radiocarbon years per 40 km, likely due to differences in upwelling strength (Robinson and Thompson 1981; McNeely et al. 1991; Jones and Jones 1992; Panich et al. 2018; Hutchinson 2020). Thus, correction for this reservoir effect is critical for accurate radiometric dating of marine samples.

In addition to spatial variability, the marine radiocarbon reservoir effect at a given location also fluctuates over time with respect to currents, vertical mixing of deep, ^{14}C-depleted water, and the volume and source of freshwater input, which in most cases mixes in ^{14}C-enriched water. However, robust estimates of the temporal variability of the marine radiocarbon reservoir effect in many regions suffer from the pooling of samples across large geographic region with differing ocean dynamics, the difficulty of sampling consistently through time at a specific location (Ascough et al. 2005; Hutchinson 2020), and the relative amount of time represented. Archaeological sites can provide some degree of repeated sampling if accurate dates can be established for terrestrial samples known to be contemporaneous with marine samples (Southon et el. 1992; Ascough et al. 2005). A relatively new approach to establishing ^{14}C variability is to sample carbonate from the absolutely dated annual increments of long-lived marine bivalves (Butler et al. 2009; Scourse et al. 2012; Wanamaker et al. 2012; Lower-Spies et al. 2020). Indeed, annual increments in bivalves can be exactly placed in time via the dendrochronology technique of crossdating to generate continuous, annually resolved, multicentennial-length chronologies. From these measurements of ^{14}C in bivalve increments, the marine radiocarbon reservoir effect can be quantified over time for the same location (Butler et al. 2009; Wanamaker et al. 2012; Lower-Spies et al. 2020). To date, this has been successfully applied in the North Atlantic to explore carbon cycling and ocean circulation by acting as a tracer of relatively "old" water depleted of ^{14}C vs. relatively "young" water more recently mingled with the atmospheric ^{14}C reservoir (Butler et al. 2009; Wanamaker et al. 2012; Lower-Spies et al. 2020).

In the northeast Pacific, temporal variability in the marine radiocarbon reservoir remains poorly quantified. To address this issue, we sample growth increments at approximately decadal intervals from a crossdated chronology of Pacific geoduck, a long-lived bivalve (*Paneopea generosa*) abundant from approximately Puget Sound, WA through Kodiak, AK, that occur from the intertidal zone to 60 meters depth. They are typically buried about 1 meter in mud-and-sand sediments and feed by extending a siphon into the water column (Goodwin 1973). Geoduck shell growth, as measured in the hinge area, is rapid in the first 10–15 years of life, declining exponentially thereafter, while year-to-year growth responds to environmental conditions, primarily water temperature (Cerrato 2000; Strom et al. 2004). The chronology was developed from samples collected near the Tree Nob Islands in northern British Columbia, Canada, and continuously spans 1725 to 2008 CE (Edge et al. 2021). Growth-increment widths from this chronology were used to develop a sea surface temperature reconstruction, which is closely tied to NE Pacific variability as reflected by a strongly positive correlation ($r = 0.62$, $p < 1.0e\text{-}5$) with the leading principal component of SST gridded data across the northeast Pacific (Edge et al. 2021). Indeed, the Tree Nob chronology has some of the strongest region-wide climate relationships of any of the network of eight geoduck chronologies developed to date (Strom et al. 2004; Black 2009; Black et al. 2010; Edge et al. 2021). Given this apparent sensitivity to regional climate variability as well as exceptional length, the Tree Nob chronology was chosen for assessing the relationships of local and basin-scale climate indicators with ^{14}C reservoir variability. We also utilized a previously published series of ^{14}C measurements (Kastelle

https://doi.org/10.1017/RDC.2022.83 Published online by Cambridge University Press

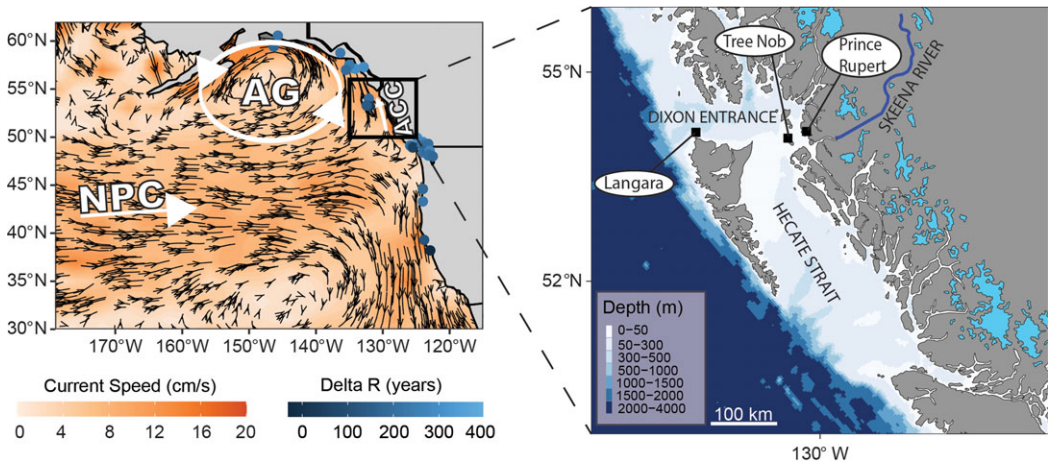

Figure 1 Study site: (a) Mixed layer ocean currents in the NE Pacific Ocean. Black streamlines indicate general surface currents based on drifting buoy data from the Atlantic Oceanographic and Meteorological Library, National Oceanic and Atmospheric Administration. Individual marine radiocarbon reservoir offset (ΔR) measurements from previous studies shown as colored points (McNeely et al. 1991; Robinson and Thompson 1981; Jones and Jones 1992; Panich et al. 2018). General location and direction of the Alaska Gyre (AG), North Pacific Current (NPC), and Alaska Coastal Current (ACC) shown in white. (b) Local bathymetry (Amante and Eakins 2009). Tree Nob geoduck collection site and measurement locations for Langara sea surface temperature and salinity (SST and SSS) and Prince Rupert sea level. Glaciers shown in bright blue. Skeena River is in dark blue. (Please see online version for color figures.)

et al. 2011) from these shells sampled through the "bomb pulse" interval (1950–1982) to provide a finer-scale assessment of the link between ^{14}C variability and instrumental climate records. In total, the pre-bomb data augments the finer-scale modern data during the bomb-pulse to provide complementary and longer-term perspectives on marine radiocarbon reservoir variability and relationships to climate and ocean dynamics.

METHODS AND BACKGROUND

Oceanographic Setting

The NE Pacific consists of a subpolar, cyclonic gyre in the Gulf of Alaska (GoA) and a subtropical, anti-cyclonic gyre (Figure 1a). The subpolar Alaska Gyre (AG) consists of the North Pacific Current (NPC) in the south and the Alaska Coastal Current (ACC) along the North American coast, which quickens and narrows west of Kodiak Island to become the Alaska Stream (Dodimead and Hollister 1958). Variability of transport within the AG is related to fluctuations in the Pacific Decadal Oscillation (PDO), the dominant mode of SST variability in the North Pacific (20–60N), and ultimately to the Aleutian Low (AL; Newman et al. 2016; Hristova et al. 2019). In addition to basin-scale phenomena, the GoA experiences local variability in the magnitude of spring runoff, up/down-welling, and mixing/stratification. Basin-scale patterns may contribute to fluctuations in the strength of the ACC, relative makeup of ACC source waters, up/down-welling in source-water regions, and vertical entrainment (Guilderson et al. 2006; Hristova et al. 2019; Hutchinson 2020). Guilderson et al. 2006) have proposed a two-end-member mixing regime for the AG based on a linear relationship between ^{14}C and potential density observed in samples collected during the summer of 2002, such that warm, ^{14}C-enriched water enters the AG from the

https://doi.org/10.1017/RDC.2022.83 Published online by Cambridge University Press

south, and the observed latitudinal gradient is due to vertical entrainment of ^{14}C depleted water within the AG.

The primary, proximate source of water at Tree Nob is from the south via Hecate Strait (HS), a shallow strait that shoals from 200 m in the south to just 50 m at its northern extent (Figure 1b). In 1983–1984 several current meters were deployed across three transects of HS, which allowed for accurate measurement of flow and the development of surrogate measures of HS flow approximated by three sea level gauges, one to the west and, two to the east ($r = 0.81$; Crawford et al. 1988). When sea level is high in the east and low in the west, geostrophic flow induces a northward current through HS.

The Tree Nob Island Group lies at the far northeastern extent of Hecate Strait. The Islands are bounded to the north by Brown Passage and to the south by Bell Passage. These waterways connect Chatham Sound, to the east, with Hecate Strait, Dixon Entrance, and the open Northeast Pacific to the west. Due to high winds and strong tides, the Tree Nob site is well mixed with the open ocean (Trites 1956; Lin and Fissel 2018). And due to strong northerly flows, Tree Nob is not strongly impacted by freshwater inputs (Lin and Fissel 2018). Although the study site lies in a quasi-estuarine environment, the strong relationship of geoduck growth increment width with regional- to basin-scale climatic indicators (Edge et al. 2021) suggests that the Tree Nob geoduck integrate environmental conditions across a broad region. Furthermore, the absolutely dated, annually resolved carbonate spans nearly three centuries to yield a marine archive with a uniquely long timespan, precision, and replication in the northeast Pacific.

Pre-Bomb Radiocarbon

Geoduck form annual increments (Shaul and Goodwin 1982), with widths highly correlated to water temperature (Strom et al. 2004; Black et al. 2009; Edge et al. 2021) that can be assigned exact calendar years through crossdating (Black et al. 2008; Kastelle et al. 2011). A crossdated chronology developed from live-collected shells in the Tree Nob Islands (Figure 1b), and later appended with dead-collected material, extends from CE 1725–2008 (Black et al. 2009; Edge et al. 2021). Live- and dead-collected shells were recovered in sand-and-mud substrate at approximately 10 m water depth. The carbonate of marine organisms is incorporated from the dissolved inorganic carbon (DIC) of ambient seawater and is thus expected to reflect local environmental conditions experienced during shell formation (Adkins et al. 2002; Beirne et al. 2012).

^{14}C samples were obtained from the Tree Nob geoduck shells over the pre-bomb chronology interval of 1725–1920. Crossdated annual increments were sampled to a depth of ~600–800 μm from the shell hinge area using a Merchantek micromill and a Brasseler USAV scriber point (item #H1621.11.008). Samples were then pooled together to obtain ~10 mg. The micromill was set to maximum drill speed, and several passes were performed ranging from 100–150 μm depth at 55 μm/s scan speed and 55 μm/s plunge speed. In total, 15 shell carbonate samples integrating ten to eleven annual increments were gathered. All samples were taken from the same cut plane used for increment-width measurement to ensure precise calendar-year dating of samples. Samples were sent to the National Ocean Sciences Accelerator Mass Spectrometry facility (NOSAMS Woods Hole, Massachusetts, USA) for ^{14}C analysis.

Laboratory derived error was provided by NOSAMS based on 10 separate measurements of each sample. NOSAMS estimates an additional error of 2.6‰ for replicate samples due to

https://doi.org/10.1017/RDC.2022.83 Published online by Cambridge University Press

variability in sample collection, processing, and homogeneity. The errors were combined to present a total measurement error of radiocarbon age (NOSAMS 2020).

ΔR is given by the difference between measured and "expected" radiocarbon age. Each milled geoduck shell sample spanned approximately 10 years, with an average date of formation which corresponds to a date on the Marine20 curve. The Marine 20 curve provides reservoir age estimates in ten-year intervals. Linear interpolation was used to better match these decadally reported radiocarbon age estimates to the average calendar year represented by each sample milled from the geoduck shells. The radiocarbon age of the sample as "expected" by Marine20 was then subtracted from the value measured by NOSAMS to give the ΔR. (Stuiver 1986b; Stuiver and Braziunas 1993; Heaton et al. 2020), where:

$$\Delta R = {}^{14}C \text{ age measured} - {}^{14}C \text{ age modeled by Marine20}$$

The Marine20 curve (Heaton et al. 2020) accounts for variability in atmospheric ^{14}C production and climate as well as interactions among the ocean, atmosphere, and biosphere. Therefore, the ΔR time series may better represent changes in local ^{14}C content than age-corrected $\Delta^{14}C$ by removing as many other sources of variability as possible.

Radiocarbon and Climate Covariability

For the pre-bomb dataset, ^{14}C values were compared by linear and polynomial regression to reconstructed, seasonal (mean Apr–Nov) sea surface temperature derived from geoduck growth-increment width as published in Edge et al. 2021). ^{14}C measurements were compared to the Northern Hemisphere (NH) volcanic explosivity index (VEI) by Pearson correlation given the likely influence of such events on ocean circulation and SST (Gao et al. 2008).

Unlike pre-bomb data, the bomb pulse ^{14}C data could be compared directly to instrumental climate records. The first of the instrumental records is sea level, which serves as a proxy for HS flow as described by Crawford et al. (1988). Data were obtained from the Canadian Hydrographic Service. Only the Prince Rupert gauge covers the full period of the bomb-pulse data and is thus the only station used, though the pairwise correlations with the other two sites suggest this gauge is representative ($r=0.949$, 0.921, 0.892; $p<0.00001$). The upwelling index, as calculated by the National Oceanic and Atmospheric Administration (NOAA) Pacific Fisheries Environmental Laboratory (PFEL) was averaged across 51°N, 131°W and 54°N, 134°W, the two stations nearest to Tree Nob. Monthly freshwater discharge from the Skeena River, just 40 km distant and the second largest river draining British Columbia, was downloaded from the Department of Environment and Natural Resources, Canada (https://wateroffice.ec.gc.ca/report/data_availability_e.html?type=historical&station=08EF001&parameter_type=Flow+and+Level). Monthly mean SST and sea surface salinity (SSS) data, collected at the Langara Lighthouse station, were obtained from Fisheries and Oceans Canada (https://open.canada.ca/data/en/dataset/719955f2-bf8e-44f7-bc26-6bd623e82884; Figure 1b). Finally, bomb-pulse ^{14}C data were compared to three basin-scale indices. Niño 3.4 is a measure of SST in the central, equatorial Pacific with strong connections to northeast Pacific SST and coastal sea surface heights (ñhttps://psl.noaa.gov/gcos_wgsp/Timeseries/Data/Niño34.long.data). The North Pacific Index is a measure of sea surface pressure in the northeast Pacific which serves as a gauge of the strength of the AL (NPI; Trenberth and Hurrell 1994; https://climatedataguide.ucar.edu/sites/default/files/npindex_monthly.txt). Finally, the PDO index (https://www.ncdc.noaa.gov/

https://doi.org/10.1017/RDC.2022.83 Published online by Cambridge University Press

teleconnections/pdo/) is the leading principal component of SSTs in the North Pacific and is closely linked to atmospheric pressure (Mantua et al. 1997; Newman et al. 2016).

Monthly climate data were averaged over 3-year intervals to match the temporal resolution of the ^{14}C sampling (Kastelle et al. 2011) such that climate data for June of 1964 were represented by the average of June 1963, 1964, and 1965 and used for comparison with the 1964-centered ^{14}C value. Correlations to the bomb-pulse ^{14}C data were performed in the R package TreeClim (Zang and Biondi 2015). Significance ($\alpha = .01$) was calculated by bootstrapping based on methods adapted from DENDROCLIM2002 (Biondi and Waikul 2004).

Bomb-Pulse Radiocarbon Data

Samples spanning the bomb-pulse period were obtained from the Tree Nob geoduck shells in a previous study (Kastelle et al. 2011). The 32 bomb-pulse samples aggregate an average of three years of growth. The age-corrected $\Delta^{14}C$ data were detrended by a latitude-specific, empirically derived marine radiocarbon curve (Helser et al. 2014) to remove the bomb signal. Given that individual, complete increments were not sampled, the mean calendar year represented by a given sample was often a decimal. To facilitate direct comparison to instrumental data, the detrended ^{14}C data were combined in three-year bins by weighted mean over the interval from 1952-1972 (Figure S1). Weights were assigned proportional to the square of the temporal proximity such that a ^{14}C datum centered at 1965.9, being 0.4 years from 1965.5, was assigned a weight of $(1.5 - 0.4)^2$.

RESULTS

Pre-Bomb Radiocarbon

The average ΔR for all pre-bomb (1725–1920) Tree Nob geoduck ^{14}C samples is +256 years ($\sigma = 22.3$ yr, n=15) and is relatively stable over time. Only one value differs from the mean by more than 2σ, corresponding to increments formed from 1802–1812 (Figure 2a; Table 1), though this sample is not an outlier with respect to the distribution of all samples based on Grubb's test (critical value=2.55, N=15, α=.05). Three samples fall outside 1σ of the mean ΔR and correspond to the years 1784–1794, 1842–1852, and 1902–1912 while all other radiocarbon ages strongly agree with Marine 20 values after ΔR adjustment.

Radiocarbon and Climate Covariability

A linear regression of ΔR onto SST with the 1802–1812 sample removed is marginally significant and has a positive slope (r^2=0.29, $p = 0.03$; Figure 2b). The 1802–1812 interval contains the most extreme SST and ^{14}C values in the record and suggests an opposing SST-radiocarbon relationship. The Tree Nob ΔR value for 1802–1812, which is greater than the mean ΔR by 2.1σ, coincides with the coldest period in the SST record reconstructed from geoduck (Figure 3). Temperatures are below 2σ between the years 1808–1812 with the lowest value in 1810 of 3.4σ below the mean. This is coincident with a volcanic eruption in late 1808 with a VEI of 5.5, though other highly explosive eruptions appear to have no relationship to Tree Nob ^{14}C (Gao et al. 2008; Guevara-Murua et al. 2014; Figure 3).

Bomb-Pulse Radiocarbon Data

Among regional climate indicators, the relationship between geoduck ^{14}C in the bomb-pulse interval and SST is perhaps the strongest and most consistent with significant and positive

https://doi.org/10.1017/RDC.2022.83 Published online by Cambridge University Press

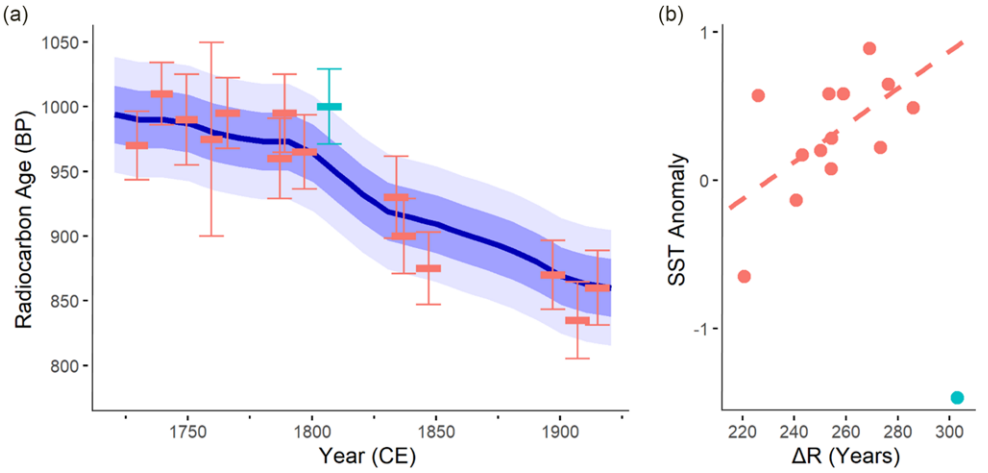

Figure 2 Pre-bomb radiocarbon: (a) Tree Nob radiocarbon ages relative to the Marine 20 curve; points above (below) line indicate older (younger) water. Red bars: radiocarbon age of Tree Nob samples that are not significantly different from Marine 20 (Heaton et al. 2020). Width of bar indicates the range of calendar years sampled. Green bar: ^{14}C sample (middle year of 1807) that is significantly different from average ΔR (2σ). See Methods for error calculation. Blue line: Average radiocarbon age for the mixed layer given by Marine20, corrected by average ΔR of all samples (+256 years). Dark blue shading: 1σ sample error of ΔR; light blue shading is 2σ. (b) ΔR vs SST. SST is the 11-year averaging of Langara SST reconstruction, z-scored (Edge et al. 2021). Coloring of points as in panel (a). Red dashed line: least squares linear fit of red points. (Please see online version for color figures.)

correlations from July through September (Figure 4). Sea level is positively correlated in February and March while Skeena River discharge negatively correlates in July and August (Figure 4). The correlation with the NOAA upwelling index is inconsistent with a significant negative relationship for February ($r=-0.77$, $p<0.01$) but a positive relationship for June ($r=0.65$, $p<0.01$) (Figure 4). The variable with strongest and most consistent relationships with geoduck ^{14}C is the Niño3.4 index, which positively correlates for almost every month from May through December and is the only variable with a significant annual relationship ($r=0.62$, $p=0.0056$; Figure 4). The NPI negatively correlates in February and September while the PDO positively correlates in February and October, suggesting young water coincident with a deeper AL and positive PDO (Figure S2).

DISCUSSION

The ΔR value at Tree Nob of 256 ± 22 years is consistent with regional measurements in both the 20th century, 249 ± 158 years (McNeely et al. 1991; http://calib.org/marine/, n=12, average distance of 280 ± 138 km, recalculated with Marine20), and throughout the Holocene, 250 ± 195 years (Schmuck et al. 2021). The Tree Nob average is also consistent with the geographically nearest 20th century measurement of 247 ± 50 (McNeely et al. 1991) and the geographically nearest archaeological site, a late-Holocene study only 30 km distant with an estimated 273 ± 38-year reservoir (Edinborough et al. 2016). These Tree Nob values fit into a broader ^{14}C gradient along the NE Pacific Coast (Figure 1a), with young water in the California Current (37–38°N, average $\Delta R = 26$ years, $\sigma = 103$ years, $n = 10$; Robinson and Thompson 1981; Ingram and Southon 1996; Panich et al. 2018), older water along Vancouver Island to the north (48–49°N, average $\Delta R = 147$ years, $\sigma = 73$ years,

https://doi.org/10.1017/RDC.2022.83 Published online by Cambridge University Press

Table 1 Radiocarbon data.

ID	$\delta^{13}C$	Sclero years	Conventional radiocarbon age	Fm	Fm error	$\Delta^{14}C$	$\Delta^{14}C$ error	ΔR	Marine20 ΔR error
OS-160307	1.52	1735–1744	1010	0.8814	0.0018	–95.87	1.85	276.31	68.32
OS-160280	0.9	1802–1812	1000	0.8829	0.0020	–101.70	2.03	303.04	65.76
OS-159180	1.45	1761–1771	995	0.8834	0.0018	–96.72	1.84	273.32	67.01
OS-157457	2.54	1784–1794	995	0.8837	0.0018	–98.92	1.84	285.94	65.25
OS-160308	1.08	1745–1754	990	0.8840	0.0030	–94.30	3.07	258.67	67.59
OS-160309	1.05	1755–1764	975	0.8856	0.0080	–93.76	8.19	250.20	67.30
OS-160306	1.89	1725–1734	970	0.8860	0.0019	–90.05	1.95	235.66	69.34
OS-159181	1.65	1792–1802	965	0.8868	0.0019	–96.63	1.94	254.20	65.22
OS-160305	1.68	1782–1792	960	0.8876	0.0019	–94.73	1.94	243.21	66.40
OS-160281	1.68	1829–1839	930	0.8910	0.0019	–96.41	1.93	269.12	66.50
OS-160282	1.39	1832–1842	900	0.8941	0.0018	–93.59	1.82	240.77	66.33
OS-160283	1.39	1842–1852	875	0.8968	0.0018	–91.96	1.82	220.79	65.74
OS-160300	1.21	1892–1902	870	0.8972	0.0018	–97.03	1.81	253.39	64.36
OS-148017	2.39	1910–1920	860	0.8985	0.0019	–97.69	1.91	254.38	63.35
OS-160301	0.86	1902–1912	835	0.9014	0.0019	–93.90	1.91	226.13	63.97

ID: Accession number. $\delta^{13}C$: measured by NOSAMS. Sclero Years: Calendar years (CE) of carbonate sample given by chronology. Conventional radiocarbon age: age (BP) based on Libby standard. Fm: Fraction modern carbon (corrected for fractionation by NOSAMS). Fm error: laboratory error reported. $\Delta^{14}C$: age-corrected based on crossdating. $\Delta^{14}C$ error: laboratory error in ‰ units. ΔR: see "Pre-Bomb Radiocarbon" section for calculation. Marine20 ΔR error: given by Marine20 (Heaton et al. 2020).

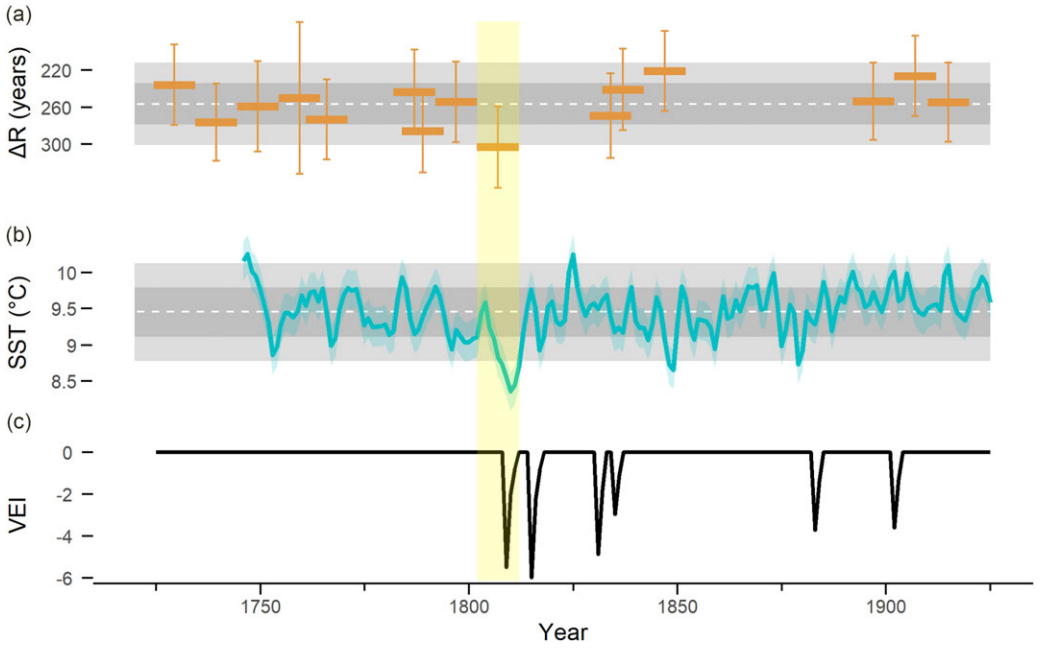

Figure 3 Tree Nob and volcanic proxy records: (a) ΔR in Tree Nob shell material; horizontal uncertainty reflects the 10–11 years represented by each sample while vertical bars are laboratory error. Dark and light gray bands indicate 1- and 2-σ from the mean (white dotted line) of Marine20. (b) Reconstructed Langara SST and 50% prediction interval from Edge et al. 2021. Dark and light gray bands indicate 1- and 2-σ from the mean (white dotted line) (c) NH VEI based on Gao et al. 2008. Yellow highlighting identifies an interval of synchronous anomalies across all three indicators and corresponds to the years 1802–1812. (Please see online version for color figures.)

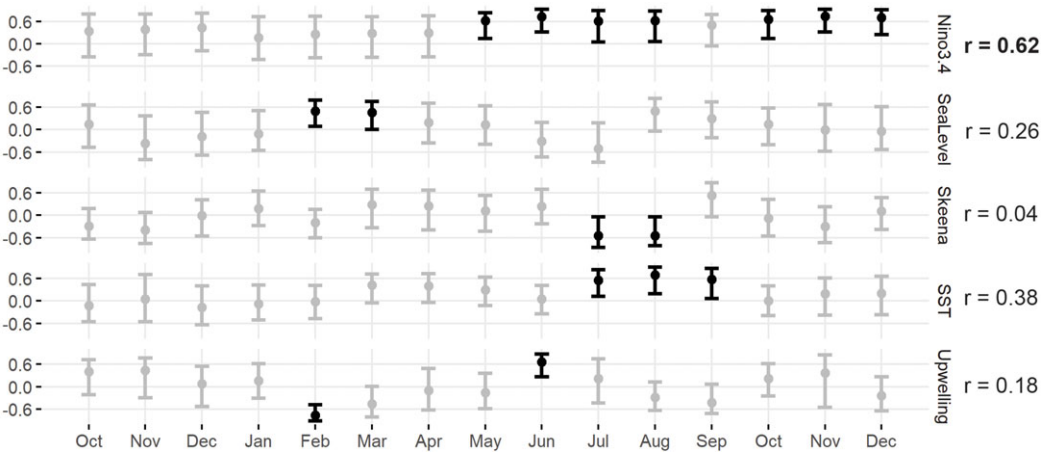

Figure 4 Bomb ^{14}C correlations with monthly-averaged climate indicators. The level of significance is $p < .01$ and is calculated by bootstrapping. Significant correlations are shown in black, non-significant in grey. Correlations with annually-averaged (Jan–Dec) climate values are shown to the right of plots, bold font indicates significance at $p < .05$. Climate data sources given in the "Radiocarbon and Climate Covariability" section.

https://doi.org/10.1017/RDC.2022.83 Published online by Cambridge University Press

n = 10; McNeely et al. 1991; Robinson and Thompson 1981), and even older water in the ACC (54–58°N, average ΔR = 346 years, σ = 83 years, n = 10; McNeely et al. 1991).

Although the Tree Nob sample site is outside the area recommended for use with the Marine20 curve given the potential impacts of sea ice (Heaton et al. 2020), the ^{14}C values observed in the geoduck increments fit remarkably well with predicted values. Indeed, ΔR showed a notable lack of variability over time, straying relatively little outside sample error estimates. The only exception is the excursion during the early 1800s for which age calculations based only on ^{14}C decay could lead to dating errors of 50 years or more (Table 1; Figures 2a and 3a). Data from elsewhere in the GoA region also suggests little variability in ΔR over the Holocene, though accuracy in these studies may be impacted by relatively small sample sizes and collections over relatively large spatial domains (Southon et al. 1990; Hutchinson 2020; Schmuck et al. 2021). Estimates of ^{14}C variability at Tree Nob of 2.9‰ in $\Delta^{14}C$ and 22 years ΔR (1σ) are also similar in magnitude to the 1σ decadal variability measured in tropical Pacific corals of 2–3‰ (e.g., Druffel 2001; Grottoli et al. 2003). This variability is much less than that of similar bivalve radiocarbon records from *Arctica islandica* shells in the North Atlantic where 1σ variability of ΔR is on the order of 40–60 years (eg. Butler et al. 2009; Wanamaker et al. 2012; Lower-Spies et al. 2020). Thus, ΔR at Tree Nob appears to be relatively stable, especially compared to published sclerochronological records from the North Atlantic, where water mass variability is likely much greater, but with the potential for significant, if infrequent, excursions as occurred in the early 1800s.

The coupled nature of the new ΔR data and existing Tree Nob geoduck growth-increment width based seasonal (Apr–Nov) SST reconstruction (Edge et al. 2021) provides a unique opportunity to evaluate the connections between marine radiocarbon and climatic variability in this region. In coastal areas currents, vertical mixing, and the volume and source of freshwater runoff may cause temporal variability in ^{14}C (Allen et al. 1995; Hickey and Banas 2008; Schmuck et al. 2021). Although instrumental records of these more proximal drivers of ^{14}C are not available prior to about 1950, SST is an environmental indicator likely influenced by some combination of these processes (Lagerloef 1995; Hristova et al. 2019). The subtle variability in ^{14}C over time, uncertainties in the ^{14}C measurements and SST estimates, and decadal averaging of all data may, in part, mask the relationship between ^{14}C and SST. Yet there was still a significant linear relationship between ΔR and SST when calculated without the highly anomalous 1802–1812 sample (Figure 2b). This relationship suggests old water is relatively warm, counter to expectations, and may represent radiocarbon-old freshwater contributions from radiocarbon-depleted glacial melt or carbonate weathering, though no substantial connections were found to river flows in the higher resolution bomb-pulse data. In contrast, the 1802–1812 datum is consistent with the expectation that colder water, often of relatively deep or more northerly origin, is depleted in ^{14}C. Indeed, anomalously old ΔR and slow geoduck growth in the early 1800s co-occurred with the most extreme cold climate event of the pre-bomb data.

The 1802–1812 ^{14}C anomaly is coincident with the largest Northern Hemisphere volcanic eruption of the Tree Nob ^{14}C period of record, the "Unknown" eruption of 1808, which led to significant cooling of the Northern Hemisphere accompanied by other climatic anomalies (Moberg et al. 2005; Gao et al. 2008; Cole-Dai et al. 2009). Climate simulations of the North Pacific response to large tropical volcanic eruptions over the last 600 years show greatly enhanced upwelling-favorable winds at Tree Nob in the years following

https://doi.org/10.1017/RDC.2022.83 Published online by Cambridge University Press

eruptions (Wang et al. 2012; Zanchettin et al. 2012). The Tree Nob region is strongly dominated by downwelling with an average annual upwelling index of –32 m^3/s per 100 m of coastline (max = –12 m^3/s/100 m, min = –69 m^3/s/100 m, 1947–2020; NOAA PFEL). Yet the 1802–1812 interval may have been associated with an anomalously strong period of upwelling, bringing cold, ^{14}C-depleted water to the surface (Wang et al. 2012; Zanchettin et al. 2012). In addition, wind reversals in the Tree Nob region evident in model simulations of the Unknown eruption may have reduced the advection of warmer, ^{14}C-enriched water into the region, further enhancing "old and cold" conditions. However, extreme ^{14}C anomalies are not evident with other major volcanic events such as Tambora or Krakatoa, possibly due to the seasonality, location, or nature of the eruptions. Thus, despite the coincidence, the relationship between extreme ^{14}C and the Unknown eruption of 1808 may be spurious. Ultimately, a mechanism for this "old and cold" event of the early 1800s cannot be identified from the radiocarbon history, though it does underscore that infrequent yet significant excursions in ^{14}C can occur and appear to be coincident with climate extremes.

The bomb-pulse ^{14}C data provides a complementary perspective on the relationship between ^{14}C and climate at somewhat finer temporal scales within an era spanned by the instrumental record. Positive correlations between SST and ^{14}C run counter to the relationship between SST and ^{14}C over the pre-bomb record and are consistent with the "old and cold" hypothesis. Bomb-pulse ^{14}C data are not significantly correlated with annual mean SST, but instead correlate during the summer months, which is when shells are most actively growing and incorporating carbonate (Shaul and Goodwin 1982; Edge et al. 2021). Beyond temperature, positive ΔR correlation with sea level suggests that the advection of water masses into the region also influences ^{14}C. High sea level anomalies indicate geostrophic flow from the south from where water is likely ^{14}C-enriched (Figure 1a). These significant correlations occur in the winter, which is when this transport is likely to be strongest (Crawford et al. 1988), moving water masses into the region that may persist into the growing season. The correlation between upwelling index and ^{14}C is also significant in the winter and could reflect the importance of vertical water movements. This region is almost exclusively dominated by downwelling, which is at its most intense during the winter months with peak mean values from November through February. The negative correlation between February upwelling and geoduck ΔR is consistent with the tendency of warmer, shallower water to be ^{14}C-enriched relative to upwelled water. The cause of the June positive correlation between upwelling and ΔR is less clear and may be spurious. One possibility is that upwelling may encourage stratification during the annual freshet, which typically peaks in June, while downwelling, especially during the annual freshet, forces lighter water under denser water to thereby enhance vertical mixing (Austin and Lentz 2002). Finally, positive correlations with Skeen River discharge in July and August, the warmest and driest months of the year, may reflect inputs of ^{14}C-depleted glacial melt. This relationship is not likely an artifact of freshwater stratification, as summer Skeena River flow is inversely correlated to local SST (r=–0.47, p=0.0078, 1940:2017 JJA Langara SST).

Correlations between basin-scale indicators and ^{14}C are consistent with those between more local indicators and ^{14}C. For example, positive Niño3.4 values indicate El Niño events, which are associated with warmer water in the region (r=0.62, p<0.00001, 1940–2017 Langara annual SST) and are thus consistent with positive correlations between ^{14}C and SST (Figure 4). Correlations with Niño3.4 persist through the growing season and beyond. However, lagged correlations into the fall are likely due to lags in climate signals from the

https://doi.org/10.1017/RDC.2022.83 Published online by Cambridge University Press

tropical Pacific, where the index is calculated, from reaching the mid-latitudes of the NE Pacific. Furthermore, modelling work demonstrates a strengthening of the ACC during El Niño events (Melsom et al. 1999), which would increase the advection of more southerly, ^{14}C-enriched water into the study region. A metanalysis of Holocene-timescale ^{14}C variability in the northeast Pacific suggests ENSO may be the most predictive climate variable for coastal ^{14}C, which is reflected by the strong correlations observed here (Hutchinson 2020). In contrast, ^{14}C correlations with PDO and NPI are considerably weaker and less consistent with ENSO. However, the nature of the correlations is consistent with overall patterns of temperature and transport in the NE Pacific. Positive values of the PDO are associated with lower atmospheric pressure over the NE Pacific and relatively strong advection of water from the south along the cost and thus through Hecate Strait. The NPI is closely related to the PDO, but more directly measures regional pressure, and is opposite in sign, explaining its negative correlation with ^{14}C relative to a positive correlation with PDO. Thus, NPI and PDO likely reflect the influence of the Aleutian Low with its ties to both AG advection (Hristova et al. 2019) and SST (Newman et al. 2016). Indeed, the intensity of the Aleutian Low is greatest in the winter, which coincides with the seasonality of the relationship with ^{14}C for both indicators.

Bomb-pulse ^{14}C are important confirmatory data for the pre-bomb but must be interpreted with caution. There may be biases in the ^{14}C bomb-pulse model used to detrend the data. Also, the bomb pulse data are from a very limited temporal window that spans a single cool regime in the North Pacific that began in 1946 and lasted through 1976 (Miller et al. 1994; Mantua et al. 1997). Thus, the bomb-pulse data lack the variability in environmental conditions covered by the pre-bomb data, absent the contrast of a warm ocean regime let alone climatic extremes such as the cold period of the early 1800s. This may help explain why the PDO, with energy in interdecadal timescales, did not correlate as strongly with the bomb-pulse data as ENSO, which has greater energy on interannual timescales. These differing temporal resolutions might also change the ^{14}C-SST relationships. Finally, the bomb-pulse itself also changes the ocean-atmosphere exchange dynamics by enhancing Δ^{14}C difference between the two reservoirs, which may affect relationships between ^{14}C and climate. Because the bomb-pulse ^{14}C time series is short (n=21) and a large number of correlation analyses were performed without a Bonferroni correction, the significance of these monthly correlations should be interpreted cautiously. Therefore, to reduce the number of spurious results, we implemented an α=.01 threshold for significance testing in TreeClim. Yet, despite these potential shortcomings, positive bomb-pulse ^{14}C correlations with SST are consistent with the "old is cold" hypothesis in which colder water masses tend to be of deeper or more northerly origin and depleted of ^{14}C. This relationship, as well as the correlations with sea level, NPI, PDO, and ENSO are also consistent with the two-end-member mixing regime proposed by Guilderson et al. 2006). Notably, this is opposite to the relationship in the pre-bomb data, wherein cold water is coincident with radiocarbon enrichment. Yet relationships between climate and ΔR are relatively weak, as is the variability in ΔR over time, suggesting that during most years radiocarbon is generally stable and minimally affected, if at all, by environmental variability at this site. The radiocarbon excursion in the early 1800s and co-occurrence with unusual cold does, however, indicate that the system is subject to anomalies consistent with the expectation of "old and cold" water masses.

Ultimately, the Tree Nob ^{14}C time series suggests ΔR is relatively stable in the decadally averaged timescales sampled here, but with the potential for significant excursions under climatic extremes such as the cold period of the early 1800s. The 1802–1812 anomaly may

https://doi.org/10.1017/RDC.2022.83 Published online by Cambridge University Press

be related to a brief, volcanic-induced climate excursion, an example of an event which may not be captured when sampling a lower temporal resolution. However, this pattern is limited to one location in the shallow nearshore environment and therefore may not well represent deeper or offshore locations. Other ^{14}C archives may better address these locations to provide a contrast for the nearshore. For example, Pacific rockfish can live for a century or longer, form annual increments that can be crossdated, and thus could provide as source of absolutely dated, offshore carbonate that would pre-date the bomb pulse (Black et al. 2008; Sydeman et al. 2014; van der Sleen 2016 POP paper). Indeed, a network of rockfish and geoduck chronologies could be sampled for ^{14}C along the NE Pacific to better quantify temporal and spatial patterns of ^{14}C variability. The timescales involved in ^{14}C analysis could also be refined if individual increments are sampled to reveal interannual variability rather than the decadal-scale resolution addressed here. Given that the Tree Nob chronology covers 58% of the past 1500 years, there is the possibility of greatly increasing the temporal depth of the ^{14}C chronology as more subfossil shells are collected to fill gaps, which could provide further insight into ^{14}C variability in the NE Pacific and potentially refine dating of other organic marine material of archaeological, geological, or climatic importance.

COMPETING INTERESTS

The authors declare no conflicts of interest.

ACKNOWLEDGMENTS

This work is funded by the National Science Foundation (AGS Award Number: 1855628 to BAB; Award Number: 1602751 to ADW).

This paper describes objective technical results and analysis. Any subjective views or opinions that might be expressed in the paper do not necessarily represent the views of the U.S. Geological Survey or the United States Government. The publisher, by accepting the article for publication, acknowledges that the United States Government retains a non-exclusive, paid-up, irrevocable, world-wide license to publish or reproduce the published form of this manuscript, or allow others to do so, for United States Government purposes.

SUPPLEMENTARY MATERIAL

To view supplementary material for this article, please visit https://doi.org/10.1017/RDC.2022.83

REFERENCES

Adkins JF, Griffin S, Kashgarian M, Cheng H, Druffel ERM, Boyle EA, et al. 2002. Radiocarbon dating of deep-sea corals. Radiocarbon 44(2):567–580. doi: 10.1017/S0033822200031921.

Allen J, Newberger P, Federiuk J. 1995. Upwelling circulation on the Oregon continental shelf. Part I: Response to idealized forcing. Journal of Physical Oceanography 25(8):1843–1866.

Alves EQ, Macario K, Ascough P, Bronk Ramsey C. 2018. The worldwide marine radiocarbon reservoir effect: Definitions, mechanisms, and prospects. Reviews of Geophysics 56: 278–305.

Amante C, Eakins BW. 2009. ETOPO1 arc-minute global relief model: procedures, data sources and analysis.

Ascough P, Cook G, Dugmore A. 2005. Methodological approaches to determining the marine radiocarbon reservoir effect. Progress in Physical Geography 29(4):532–547.

Austin JA, Lentz SJ. 2002. The inner shelf response to wind-driven upwelling and downwelling. Journal of Physical Oceanography 32(7):2171–2193.

Beirne EC, Wanamaker AD, Feindel SC. 2012. Experimental validation of environmental controls on the $\delta^{13}C$ of Arctica islandica (ocean quahog) shell carbonate. Geochimica et Cosmochimica Acta 84:395–409. doi: 10.1016/j.gca.2012.01.021.

Biondi F, Waikul K. 2004. DENDROCLIM2002: A C++ program for statistical calibration of climate signals in tree-ring chronologies. Computers & Geosciences 30(3):303–311.

Black BA, Copenheaver CA, Frank DC, Stuckey MJ, Kormanyos RE. 2009. Multi-proxy reconstructions of northeastern Pacific sea surface temperature data from trees and Pacific geoduck. Palaeogeography, Palaeoclimatology, Palaeoecology 278(1–4):40–47.

Black BA, Dunham JB, Blundon BW, Raggon MF, Zima D. 2010. Spatial variability in growth-increment chronologies of long-lived freshwater mussels: implications for climate impacts and reconstructions. Ecoscience 17(3):240–250.

Black BA, Gillespie DC, MacLellan SE, Hand CM. 2008. Establishing highly accurate production-age data using the tree-ring technique of crossdating: a case study for Pacific geoduck (Panopea abrupta). Canadian Journal of Fisheries and Aquatic Sciences 65(12):2572–2578.

Büntgen U, Wacker L, Galván JD, Arnold S, Arseneault D, Baillie M, Beer J, Bernabei M, Bleicher N, Boswijk G. 2018. Tree rings reveal globally coherent signature of cosmogenic radiocarbon events in 774 and 993 CE. Nature Communications 9(1):1–7.

Butler PG, Scourse JD, Richardson CA, Wanamaker Jr, AD, Bryant CL, Bennell JD. 2009. Continuous marine radiocarbon reservoir calibration and the ^{13}C Suess effect in the Irish Sea: results from the first multi-centennial shell-based marine master chronology. Earth and Planetary Science Letters 279(3–4):230–241.

Cerrato RM. 2000. What fish biologists should know about bivalve shells. Fisheries Research 46(1–3):39–49.

Cole-Dai J, Ferris D, Lanciki A, Savarino J, Baroni M, Thiemens MH. 2009. Cold decade (AD 1810–1819) caused by Tambora (1815) and another (1809) stratospheric volcanic eruption. Geophysical Research Letters, 36:22.

Crawford WR, Huggett WS, Woodward MJ. 1988. Water transport through Hecate Strait, British Columbia. Atmosphere-Ocean 26(3):301–320.

Dodimead A, Hollister H. 1958. Progress report of drift bottle releases in the northeast Pacific Ocean. Journal of the Fisheries Board of Canada 15(5):851–865.

Druffel ER, Griffin S, Guilderson T, Kashgarian M, Southon J, Schrag D. 2001. Changes of subtropical North Pacific radiocarbon and correlation with climate variability. Radiocarbon 43(1):15–25.

Edge DC, Reynolds DJ, Wanamaker AD, Griffin D, Bureau D, Outridge C, Stevick BC, Weng R, Black BA. 2021. A multicentennial proxy record of northeast Pacific Sea surface temperatures from the annual growth increments of Panopea generosa. Paleoceanography and Paleoclimatology 36(9): e2021PA004291.

Edinborough K, Martindale A, Cook GT, Supernant K, Ames KM. 2016. A marine reservoir effect ΔR value for kitandach, in Prince Rupert Harbour, British Columbia, Canada. Radiocarbon 58(4):885–891.

Gao C, Robock A, Ammann C. 2008. Volcanic forcing of climate over the past 1500 years: an improved ice core-based index for climate models. Journal of Geophysical Research: Atmospheres 113:D23.

Goodwin CL. 1973. Subtidal geoducks of Puget Sound, Washington. Wash. Dept. Fish. Tech. Rep. 13. 64 p.

Grottoli A, Gille S, Druffel ER, Dunbar R. 2003. Decadal timescale shift in the 14C record of a central equatorial Pacific coral. Radiocarbon 45(1):91–99.

Guevara-Murua A, Williams CA, Hendy EJ, Rust AC, Cashman KV. 2014. Observations of a stratospheric aerosol veil from a tropical volcanic eruption in December 1808: is this the Unknown 1809 eruption? Climate of the Past 10(5):1707–1722.

Guilderson TP, Roark EB, Quay PD, Page SRF, Moy C. 2006. Seawater radiocarbon evolution in the Gulf of Alaska: 2002 observations. Radiocarbon 48(1):1–15.

Heaton TJ, Köhler P, Butzin M, Bard E, Reimer RW, Austin WE, Ramsey CB, Grootes PM, Hughen KA, Kromer B. 2020. Marine20—the marine radiocarbon age calibration curve (0–55,000 cal BP). Radiocarbon 62(4):779–820.

Helser TE, Kastelle CR, Lai H-l. 2014. Modeling environmental factors affecting assimilation of bomb-produced $\Delta^{14}C$ in the North Pacific Ocean: implications for age validation studies. Ecological Modelling 277:108–118.

Hickey BM, Banas NS. 2008. Why is the northern end of the California Current System so productive? Oceanography 21(4):90–107.

Hristova HG, Ladd C, Stabeno PJ. 2019. Variability and trends of the Alaska Gyre from Argo and satellite altimetry. Journal of Geophysical Research: Oceans 124(8):5870–5887.

Hutchinson I. 2020. Spatiotemporal variation in ΔR on the West Coast of North America in the late Holocene: implications for dating the shells of marine mollusks. American Antiquity, 85(4):676–693.

Ingram BL, Southon JR. 1996. Reservoir ages in eastern Pacific coastal and estuarine waters. Radiocarbon 38(3):573–582.

https://doi.org/10.1017/RDC.2022.83 Published online by Cambridge University Press

Jones TL, Jones DA. 1992. Elkhorn Slough revisited: reassessing the chronology of CA-MNT-229. Journal of California and Great Basin Anthropology 14(2):159–179.

Kastelle CR, Helser TE, Black BA, Stuckey MJ, Gillespie DC, McArthur J, Little D, Charles KD, Khan RS. 2011. Bomb-produced radiocarbon validation of growth-increment crossdating allows marine paleoclimate reconstruction. Palaeogeography, Palaeoclimatology, Palaeoecology 311(1–2): 126–135.

Lagerloef GS. 1995. Interdecadal variations in the Alaska Gyre. Journal of Physical Oceanography 25(10):2242–2258.

Lower-Spies EE, Whitney NM, Wanamaker AD, Griffin SM, Introne DS, Kreutz KJ. 2020. A 250-year, decadally resolved, radiocarbon time history in the Gulf of Maine reveals a hydrographic regime shift at the end of the Little Ice Age. Journal of Geophysical Research: Oceans 125(9):e2020JC016579.

Lin Y, Fissel DB. 2018. The ocean circulation of Chatham Sound, British Columbia, Canada: Results from numerical modelling studies using historical datasets. Atmosphere-Ocean, 56(3):129–151.

Mantua NJ, Hare SR, Zhang Y, Wallace JM, Francis RC. 1997. A Pacific interdecadal climate oscillation with impacts on salmon production. Bulletin of the American Meteorological Society 78(6):1069–1080.

McNeely R, McCuaig S. 1991. Geological Survey of Canada radiocarbon dates XXIX.

Melsom A, Meyers SD, O'Brien JJ, Hurlbur, HE, Metzger JE. 1999. ENSO effects on Gulf of Alaska eddies. Earth Interactions 3(1):1–30.

Miller AJ, Cayan DR, Barnett TP, Graham NE, Oberhuber JM. 1994. The 1976–77 climate shift of the Pacific Ocean. Oceanography 7(1):21–26.

Moberg A, Sonechkin DM, Holmgren K, Datsenko NM, Karlén W. 2005. Highly variable Northern Hemisphere temperatures reconstructed from low-and high-resolution proxy data. Nature 433(7026):613–617.

Newman M, Alexander MA, Ault TR, Cobb KM, Deser C, Di Lorenzo E, Mantua NJ, Miller AJ, Minobe S, Nakamura H. 2016. The Pacific decadal oscillation, revisited. Journal of Climate 29(12):4399–4427.

NOSAMS. 2020. Radiocarbon Data and Calculations. National Ocean Sciences Accelerator Mass Spectrometry. https://www2.whoi.edu/site/nosams/client-services/radiocarbon-data-calculations/

Panich LM, Schneider TD, Engel P. 2018. The marine radiocarbon reservoir effect in Tomales Bay, California. Radiocarbon 60(3):963–974.

Pearson C, Salzer M, Wacker L, Brewer P, Sookdeo A, Kuniholm P. 2020. Securing timelines in the ancient Mediterranean using multiproxy annual tree-ring data. Proceedings of the National Academy of Sciences 117(15):8410–8415.

Reimer PJ, Austin WE, Bard E, Bayliss A, Blackwell PG, Ramsey CB, Butzin M, Cheng H, Edwards RL, Friedrich M, et al. 2020. The IntCal20 Northern Hemisphere radiocarbon age calibration curve (0–55 cal kBP). Radiocarbon 62(4):725–757.

Robinson SW, Thompson G. 1981. Radiocarbon corrections for marine shell dates with application to southern Pacific Northwest Coast prehistory. Syesis 14:45–57.

Schmuck N, Reuther J, Baichtal JF, Carlson RJ. 2021. Quantifying marine reservoir effect variability along the Northwest Coast of North America. Quaternary Research:1–22.

Schuur EA, Druffel ER, Trumbore SE. 2016. Radiocarbon and climate change: Mechanisms, applications and laboratory techniques. Springer.

Scourse JD, Wanamaker AD, Weidman C, Heinemeier J, Reimer PJ, Butler PG, et al. 2012. The marine radiocarbon bomb pulse across the temperate North Atlantic: a compilation of $\Delta^{14}C$ time histories from Arctica islandica growth increments. Radiocarbon 54(2):165–186.

Shaul W, Goodwin L. 1982. Geodock (Panope generosa: Bivalvia) age as determined by internal growth lines in the shell. Canadian Journal of Fisheries and Aquatic Sciences 39(4):632–636.

Southon JR, Nelson DE, Vogel JS. 1990. A record of past ocean–atmosphere radiocarbon differences from the northeast Pacific. Paleoceanography 5(2):197–206.

Southon J, Nelson D, Vogel J. 1992. The determination of past ocean-atmosphere radiocarbon differences. NATO advanced research workshop on the last deglaciation: absolute and radiocarbon chronologies.

Strom A, Francis RC, Mantua NJ, Miles EL, Peterson DL. 2004. North Pacific climate recorded in growth rings of geoduck clams: a new tool for paleoenvironmental reconstruction. Geophysical Research Letters 31:6.

Stuiver M, Braziunas TF. 1993. Modeling atmospheric ^{14}C influences and ^{14}C ages of marine samples to 10,000 BC. Radiocarbon 35(1):137–189.

Stuiver M, Kromer B, Becker B, Ferguson CW. 1986a. Radiocarbon age calibration back to 13,300 years BP and the ^{14}C age matching of the German oak and US bristlecone pine chronologies. Radiocarbon 28(2B):969–979.

Stuiver M, Pearson GW, Braziunas T. 1986b. Radiocarbon age calibration of marine samples back to 9000 cal yr BP. Radiocarbon 28(2B):980–1021.

Sydeman W, García-Reyes M, Schoeman DS, Rykaczewski R, Thompson S, Black B, Bograd S. 2014. Climate change and wind

https://doi.org/10.1017/RDC.2022.83 Published online by Cambridge University Press

intensification in coastal upwelling ecosystems. Science 345(6192):77–80.
Trenberth KE, Hurrell JW. 1994. Decadal atmosphere-ocean variations in the Pacific. Climate Dynamics 9(6):303–319.
Trites RW. 1956. The oceanography of Chatham Sound, British Columbia. Journal of the Fisheries Board of Canada 13(3):385–434.
van der Sleen P, Dzaugis MP, Gentry C, Hall WP, Hamilton V, Helser TE, Matta ME, Underwood CA, Zuercher R, Black BA. 2016. Long-term Bering Sea environmental variability revealed by a centennial-length biochronology of Pacific Ocean perch Sebastes alutus. Climate Research 71(1):33–45.
Wanamaker AD, Butler PG, Scourse JD, Heinemeier J, Eiríksson J, Knudsen KL, Richardson CA. 2012. Surface changes in the North Atlantic meridional overturning circulation during the last millennium. Nature Communications 3(1):1–7.
Wang T, Otterå OH, Gao Y, Wang H. 2012. The response of the North Pacific Decadal variability to strong tropical volcanic eruptions. Climate Dynamics 39(12):2917–2936.
Zanchettin D, Timmreck C, Graf H-F, Rubino A, Lorenz S, Lohmann K, Krüger K, Jungclaus J. 2012. Bi-decadal variability excited in the coupled ocean–atmosphere system by strong tropical volcanic eruptions. Climate Dynamics 39(1):419–444.
Zang C, Biondi F. 2015. treeclim: an R package for the numerical calibration of proxy-climate relationships. Ecography 38(4):431–436.

https://doi.org/10.1017/RDC.2022.83 Published online by Cambridge University Press